CFD Letters

Journal homepage:
https://semarakilmu.com.my/journals/index.php/CFD_Letters/index
ISSN: 2180-1363

Numerical and Experimental Investigations into the Characteristics of Wageningen B4-70 Series of Propeller with Boss Cap Fins

Berlian Arswendo Adietya[1], I Ketut Aria Pria Utama[1,*], Wasis Dwi Aryawan[1], Mochammad Nasir[2], Nurcholis[2], Mahendra Indiaryanto[2], Nurwidhi Asrowibowo[2], Rizqi Dian Permana[2], Nurhadi[2]

[1] Department of Naval Architecture, Faculty of Marine Technology, Institut Teknologi Sepuluh Nopember (ITS), Surabaya 60111, Indonesia
[2] Research Center for Hydrodynamics Technology, National Research and Innovation Agency (BRIN), Surabaya 60117, Indonesia

ARTICLE INFO

Article history:
Received 28 March 2023
Received in revised form 25 April 2023
Accepted 20 May 2023
Available online 1 October 2023

Keywords:
B4-70; CFD; Energy Efficiency; PBCF; RANSE

ABSTRACT

Applying propeller boss cap fins (PBCF) in open B-series has been studied. PBCF is able to decrease the wake effect behind the propeller which can influence the propeller's thrust and torque. Open propeller using PBCF is analyzed using computational fluid dynamics (CFD) which generate convergent result compared to experimental data. The solver is based on the Reynolds Averaged Navier Stokes Equation (RANSE) solutions and turbulence modeling explicit algebraic stress model (EASM). The test data was obtained from CFD simulations consisting of the open propeller and PBCF despite the experiment was done to PBCF only. All measurements were carried out from J = 0 to J = 1.0 with speeds from 0 m/s to 2.445 m/s.The results of the investigation on the B4-70 propeller with Boss cap fins convergent showed thought-provoking phenomena both on CFD and experimental work. Test results at The B4-70 Propeller without using PBCF high Pressure at J = 0.1 - 0.9, but with boss cap fins can reduce pressure at high-speed J = 0.9, so further research is needed to low-speed J = 0.1 - 0.5; Then visualization of velocity on propeller B4-70 without PBCF shows an increase in flow velocity in the boss cap fins when J = 0 to J = 0.9. The induced axial velocity in the blade propeller is the same and propeller B4-70 with PBCF decreases in speed in the boss cap fins when J = 0 to J = 0.9. However, the induce axial velocity in the blade propeller is the same. Convergent PBCF can reduce the return flow velocity in the boss cap propeller area, inversely proportional to the open propeller. Comparison of open propeller and PBCF shows that using PBCF there is an increase in the K_T value at high speed of 10% to24% and a decrease in the $10K_Q$ value on PBCF from J = 0.8 to J = 1.0 of 7% to 14%, but η_0 value at J = 0.8 to J = 1.0 increased by 3% to 8%. This Explained that the use of PBCF when the higher the value of J, greater the increase in η_0 value. Mainly, B4-70 propeller with PBCF with a converging boss cap shape with 15-degree slope exhibits increased efficiency.

1. Introduction

In 2023, the global economy is failing, as shown by the decrease in public spending capability, which has led to demand reduction [1]. However, the ship requirements to follow shipping rules and

* *Corresponding author.*
E-mail address: kutama@na.its.ac.id (I Ketut Aria Pria Utama)

https://doi.org/10.37934/cfdl.15.10.152169

regulations increase operational costs. As academics seek to improve propeller performance, shipping corporations need to cut expenses. Installation of an Energy Saving Device (ESD) is one of the solutions. Several studies indicate that installing an ESD aboard a ship can impact a substantial increase in the efficiency of energy [2]. With improved computational devices and advanced numerical method software, optimization processes are becoming increasingly popular for maximizing the efficiency of energy potential in this device which is caused by changing the design.

However, these solutions may be too disruptive for retrofitting and the adoption of ESD, whose installation does not require significant hull and/or rudder modifications, or stator fins, resulting in compliance with the Energy Efficiency Operation Index (EEOI) requirements that is preferable in the case of already operational ships [3-5]. Propeller Boss Cap Fins (PBCF) are one of the most used ESD components. It consists of several fins (usually the same number as the number of propeller blades) that are attached to the hub boss cap with a very small angle of attack. Their installation is the least expensive and most straightforward, requiring only the change of the hubcap. According to prior Computational Fluid Dynamics (CFD) based research, B-series propellers perform much better as open propellers (both by default and with PBCF), whereas Kaplan series propellers perform particularly well when paired with ducted [6]. The hydrodynamic performance was determined using CFD analysis in the present work such as turbulent parameters and flow rate effect on the propeller [7,8]. After a study on the open propeller types B-Series and Kaplan has been carried out, the PBCF and Ducted propeller types were combined. To investigate the effect of PBCF and Ducted on the hydrodynamic performance of propulsion, flow field distributions were incorporated into numerical simulations.

The explicit algebraic stress model (EASM) model aims at providing better prediction compared with the linear eddy-viscosity model, rather than to avoid singularity in turbulence modelization which is inexistent for almost all turbulence models in past years, emerging as a big area of turbulence model research [9]. In a seasoned two-equation turbulence model, the Reynolds stress was obtained by converting the turbulent model equation's differential form to a strictly explicit algebraic expression, which was then enhanced by an explicit nonlinear Reynolds stress term. It is a nonlinear algebraic stress model that makes use of the eddy viscosity assumption. EASM has several benefits, including greater numerical effectiveness in comparison to the algebraic Reynolds stress model (ARSM), the ability to overcome a few shortcomings of the linear eddy viscosity model, reflect the anisotropy effect of Reynolds stress, effectively avoid numerical singularity, and improve model stability and more efficient CPU usage compared to Reynold Stress Turbulence Model (RSTM) [10].

This research includes numerical and experimental comparisons of open Propellers with PBCF, as well as case studies using B4-70 propeller. The analysis was carried out numerically by CFD method. For turbulence modeling, the solver is based on Reynolds Averaged Navier Stokes Equation (RANSE) solutions and an explicit algebraic stress model (EASM).

2. Methodology

Propeller performance is calculated by the numerical CFD method that is calculated by several criteria consisting of thrust (K_T) and torque (K_Q) coefficients and efficiency (η_0).

2.1 Modeling

Table 1 shows the main dimension of the scaled propeller which used B-series with PBCF Convergent.

Table 1
Main dimension of propeller

Type	Unit	B-Series
Dimension (D)	mm	300
The Number of Blades	-	4
Expanded area ratio (Ae/Ao)	-	0.7
Pitch of ratio	-	1.2
Angular Velocity	rpm	489

Among others, the selection of fins using the Sobol design [11] as shown in Table 2 showed an increase in the net energy efficiency of 1.3%. So that it can be used as a reference for the use of boss cap fins to increase efficiency on the B4-70 propeller.

Table 2
Sample of Sobol design number 30 [11]

Fin Height	Fin Length	Pitch	Start Angle
0.08 m	0.64 m	28.1°	33,3°

Figure 1(a) explains the CFD test model with the model scale size and Figure 1(b) the experimental test model with the model scale size. In the model in Figure 1, the propeller B4-70 is installed with PBCF Convergent which is subjected to an open water test with the output value of thrust and torque hence it can calculate the efficiency value that occurs.

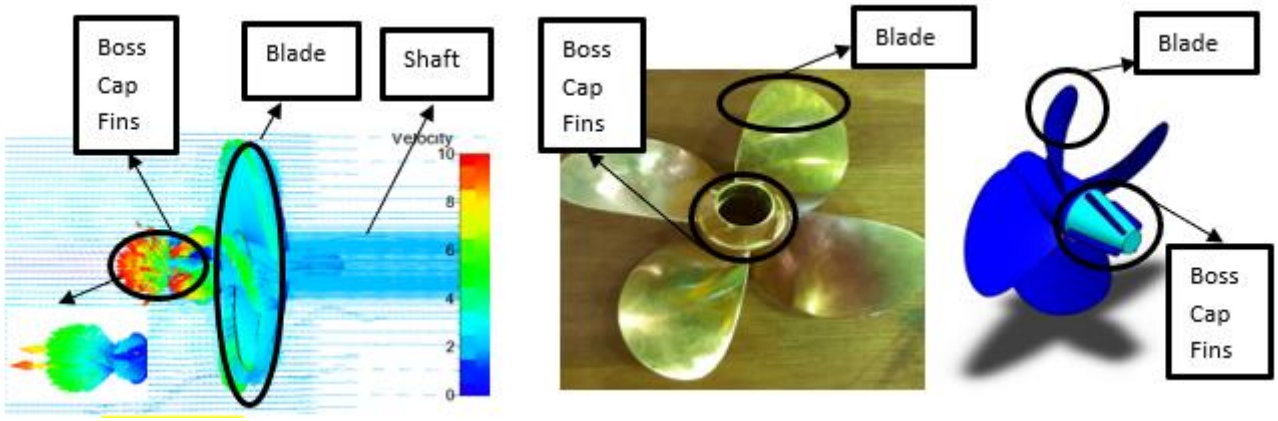

(a) (b)

Fig. 1. B4-70 test model with PBCF Convergent (a) CFD model (b) Experiment model

2.2 Numerical Simulation

Numerical simulation provides an explanation including the governing equation which describes the equations of the continuity equation, the Reynolds-Averaged Navier-Stokes Equation (RANSE), and EASM; boundary condition describes the shape of the boundary between the propeller and the environment, grid generation describes that the shape of the grid in meshing meets convergence and grid independence.

2.2.1 Governing equations

The numerical CFD method was applied to calculate the model resistance. Kawamura *et al.,* [12] researched CFD simulation of PBCF and described that lower error between numerical and

experiment. The numerical simulation is carried out using continuity equation into unsteady conditions, Reynolds-Averaged Navier-Stokes Equation (RANSE), and EASM to solve the turbulence phenomena [13]. The equations for those three are shown in Eq. (1) to Eq. (3), respectively

$$\frac{\partial \rho}{\partial t} + \frac{\partial (\rho u)}{\partial x} + \frac{\partial (\rho v)}{\partial y} + \frac{\partial (\rho w)}{\partial z} = 0 \quad (1)$$

Where: ρ is the density of the fluid, t represents the time, while u, v, and w is the vector field of flow speed.

$$\frac{\partial U_i}{\partial t} + U_j \frac{\partial U_j}{\partial X_j} = \frac{\partial p}{\partial X_i} + \frac{\partial}{\partial X_j}\left[Re_{eff}^{-1}\left(\frac{\partial U_i}{\partial X_j} + \frac{\partial U_j}{\partial X_i}\right)\right] + \frac{1}{2}\left(\frac{\partial U_i}{\partial X_j} + \frac{\partial U_j}{\partial X_i}\right) \quad (2)$$

Where U_i = (u, v, w) denoted Reynolds average velocity components; x_i = (x, y, z) denoted the independent coordinate direction; S_i symbolized the mean strain-rate tensor for a body force; *p* is the piezometric pressure, and Re_{eff} denoted effective Reynolds numbers.

The Reynolds stress in Eq. (2) is modelized with the EASM model. The EASM model's mathematical foundation and detailed derivation are taking references to previous studies [4-7,14] and describing the final result of the Algebraic Reynolds Stress Model for two-dimensional flow, which is briefly repeated here for completeness. The Reynolds stress tensor is calculated as follows:

$$\tau_{IJ} = 2vt\left(S_{ij} - \frac{1}{3}\frac{\delta_{uk}}{\delta_{xk}}\delta_{ij} + \left[a_2 a_4\left(S_{Ik}W_{kj} - W_{ik}S_{kj}\right) - 2_{a3a4}\left(S_{ik}S_{kj} - \frac{1}{3}S_{kl}S_{lk}\delta_{ij}\right)\right]\right) - \frac{2}{3}\rho k\delta_{ij} \quad (3)$$

The turbulent eddy viscosity is determined from:

$$v_t = \frac{2}{3}k\delta_{IJ} + max(-k_{\alpha 1}, 0.0005\frac{k^2}{\epsilon}) \quad (4)$$

Where α is obtained from the solution of the following cubic equation:

$$(\alpha_1/\tau)^3 + p(\alpha_1/\tau)^2 + q(\alpha_1/\tau) + r = 0 \quad (5)$$

Where τ = k/ϵ is turbulence time scale, and:

$$p = -\frac{\gamma_1}{\eta^2\tau^2\gamma_0}, p = \frac{1}{(2\eta^2\tau^2\gamma_0)^2}(\gamma_1^2 - 2\eta^2\tau^2\gamma_0 a_1 - \frac{2}{3}\eta^2\tau^2\alpha_3^2 + 2R^2\eta^2\tau^2\alpha_2^2), r = \frac{\gamma_1}{(2\eta^2\tau^2\gamma_0)^2} \quad (6)$$

In addition, it is used the compose the Reynold stress into a linear part and a residual part according to

$$\tau_{ij} = \left(\frac{2}{3}k\delta_{IJ} + 2vtS_{IJ}\right) + \tau_{ij}^r \text{ with } \tau_{ij}^r = \tau_{ij}^{asm} - \frac{2}{3}k\delta_{IJ} + 2vtS_{IJ} \quad (7)$$

Where is τ_{ij}^{asm} obtained from algebraic stress equation (ASM), v_t is eddy viscosity, and k is kinematics.

2.2.2 Boundary condition

This study explains that the boundary conditions of the b-series propeller are presented in Figure 2 and the particulars of the two domains can be seen in Table 3

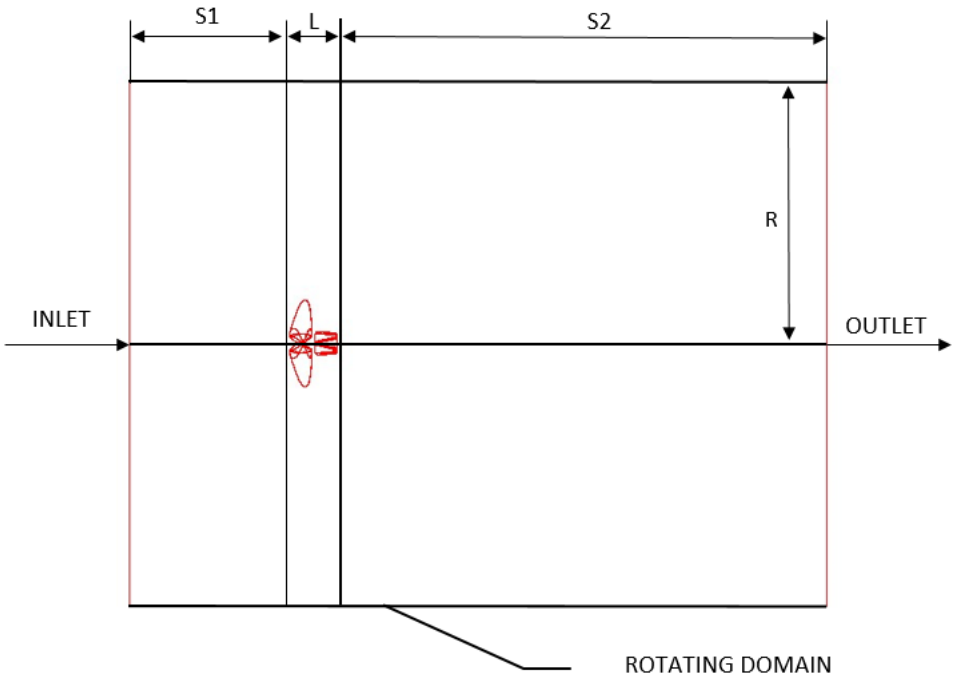

Fig. 2. Boundary conditions

Table 3
Distance of the model to the domain boundary

Location	Distances
(D) Propeller diameter	300 mm
(S1) Distances from propeller to the inlet	2D
(S2) Distances from propeller to outlet	6D
(R) The distances from the propeller center to the wall	3D
(L) Propeller length from hub to boss cap fins	0.6D

The inlet boundary condition is defined as the far field. At the outlet boundary, Prescribed Pressure is used as the boundary condition. No-slipping is defined as a boundary condition in the Solid Model. The Far Field boundary conditions are applied to the cylindrical surface so that the entire domain is the rotating domain. The rotating frame must be large enough to avoid the Far Field Boundary affecting the prediction of flow around the propeller. Meanwhile, the intended domain is a cylinder with a length and diameter of 8D and 6D respectively with the axis that coincides with the propeller's axis of symmetry. The inlet is located 2D from the model and the outlet is located 6D from the model.

2.2.3 Grid generation

CFD Design was used to create the mesh, which can be seen in Figure 3. The use of good meshing should ensure the adequacy of CFD calculations [15]. To achieve this, it is necessary to study grid independence. The adequacy of the number of meshing describes the working hours of computer

calculations to be effective and optimal [16]. In addition, the selection of meshing forms and their arrangement influences the simulation results obtained. The selection of the mesh structure is proven to generate good results in CFD simulations. Simulation precision can be improve by providing finer grid around the model that interacts with the fluid so that interaction phenomena can be shown properly. Meanwhile, in the distant part of the fluid, it can be arranged with larger grid elements to reduce the process of calculating CFD simulations. This setting provides more effective computer performance and accuracy results.

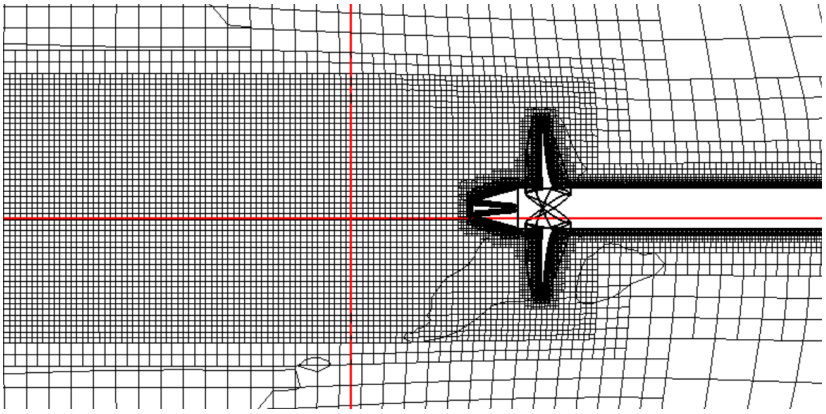

Fig. 3. Meshing of propeller model B4-70 with PBCF Convergent

Additionally, an independence grid is added to the several elements to get a constant number which can influence lower error as shown in Figure 4. Comparing numerical and experimental indicate the error number is below 2% [17]. However, the value of <0,5% is preferred in the Table 4

Table 4
Grid independence propeller B4-70 with PBCF Convergent

Number of Element	512,798	1,005,782	2,219,443	4,506,342
K_T	0.264	0.247	0.237	0.234
Percentage	-	1.8%	1.0%	0.3%

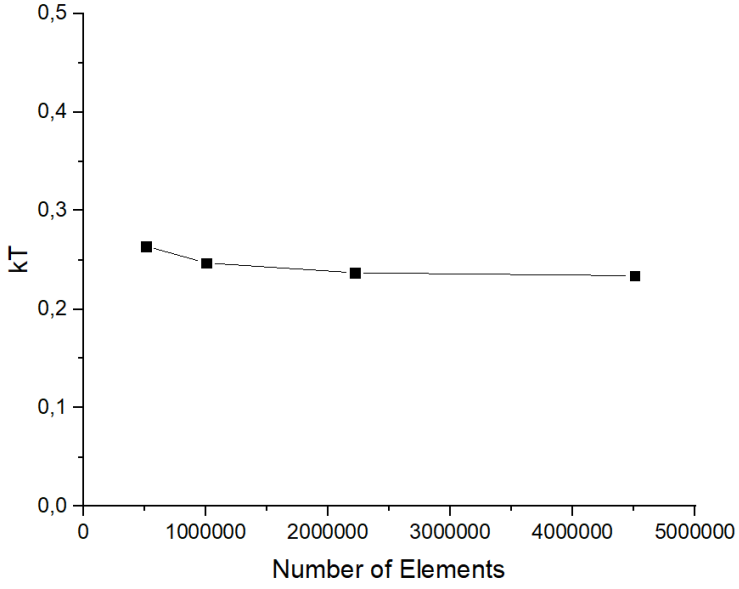

Fig. 4. Grid independence propeller B4-70 with PBCF Convergent for kT

2.3 Towing Test Model

The laboratory parameters for testing the propeller model must be considered and adjusted to the capacity and carriage equipment [18]. The test model must have strong material and precise size. For this reason, before testing, a balancing model is usually carried out on each blade in order to get the same weight on each blade.

The experimental test was carried out using a towing tank belonging to LHI situated in Surabaya Indonesia, with particulars: length = 234.5 meters, width = 11 meters, depth = 5.5 m, the maximum speed of carriage = 8 m/s, maximum acceleration of carriage = 1 m/s^2, ship model length = 3 - 9 m. Figure 5 showed the physics of the towing tank.

Fig. 5. Towing tank at Indonesian Hydrodynamic Laboratory (LHI)

Figure 6 shows the open water test and Figure 7 shows the working system in towing tank for open water test respectively. Explanation of the working system for the open water test [19] is as follows: (i) the dynamometer (H-39) is a measuring instrument used to carry out open water testing, where the sensor attached to the dynamometer is based on strain gages. This dynamometer converts the thrust and torque from the tested propeller (microstrain) or into mv/volt electricity, (ii) Programmable Signal Conditioning (PSC) that functions as a signal conditioner for the amount of thrust and torque generated by the dynamometer. So in this PSC, there is a sensor voltage source, as well as gain settings and filter signals generated by the dynamometer so that they become electrical measurements, (iii) Data Acquisition System (DAS) is a data retrieval system from sensors that have been converted to electrical signals in the PSC, then converted to digital numbers according to the calibration factor (voltage to torque thrust ratio) which will be stored in the computer for further processing and analysis.

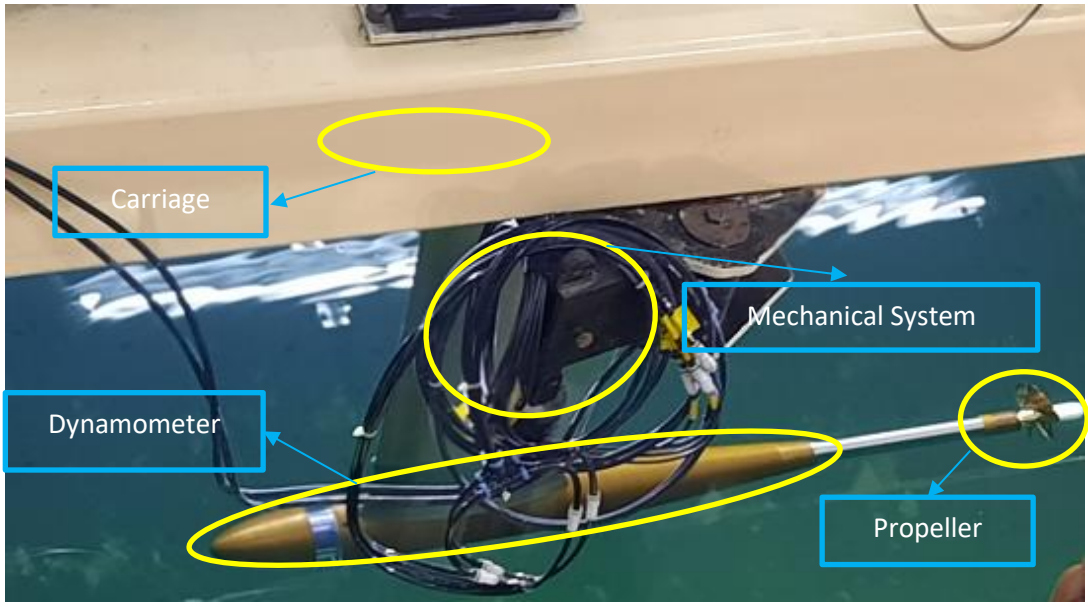

Fig. 6. Open water test

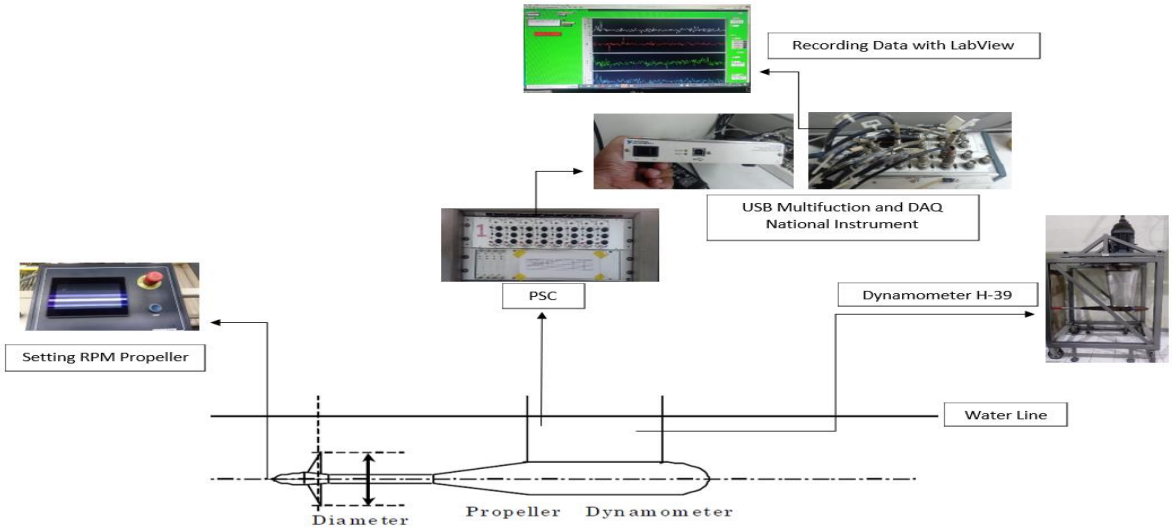

Fig. 7. Working system in towing tank for open water test

2.4 Propeller Efficiency

A propeller is typically mounted on a ship's stern so that it may operate in water that the ship encounter as it sails. So, the ship to which the propeller is mounted has an impact on its performance. So, it is required to operate the propeller in open water in order to evaluate the fundamental performance characteristics of a propeller, independent of the ship to which it is connected. A propeller's performance characteristics typically refer to the difference in its thrust, torque, and efficiency with advanced speed and rotation rate in open water. Experiments are carried out with models of the propeller that are towed in the towing tank while changing the rotation rate and towing velocity to determine the characteristics of the propeller in open water. The propeller's thrust and torque are calculated. The non-dimensional thrust K_T and torque K_Q (which is magnified 10 times as $10k_Q$ to be plotted in the same graph) are then plotted as a function of advance coefficient J, along with open water efficiency η_0. Eq. (8) to Eq. (11) show the formulation of J, K_T, K_Q, η_0.

$$J = \frac{V_A}{nD} \tag{8}$$

$$K_T = \frac{T}{\rho n^2 D^4} \tag{9}$$

$$K_Q = \frac{Q}{\rho n^2 D^5} \tag{10}$$

$$\eta_0 = \frac{v_a}{2\pi nD}\frac{K_T}{K_Q} \tag{11}$$

3. Results and Discussion

The results of the B4-70 Propeller CFD with and without PBCF Convergent calculations are shown in Table 5 and Table 6, While the results of the B4-70 Propeller Experiment with PBCF Convergent can be seen in Table 7. Moreover, a comparison of the results between the CFD and Experiment can be seen in Figure 8(a), Figure 8(b), and Figure 8(c).

Open water test propeller model was carried out in calm water conditions in accordance with ITTC regulations for open-water tests [20]. The test results can present the value of K_T, $10K_Q$, and η_0 of CFD simulations and experiments. Comparison of B4-70 propeller without PBCF Convergent can be seen in Table 5 and Table 6 namely B4-70 propeller with PBCF Convergent, when without PBCF J = 0.1 K_T value is 0.527; J = 0.5 K_T value 0.370; J = 0.9 K_T value (0.159) compared to PBCF when J = 0.1 K_T value is 0.526; J = 0.5 K_T value 0.373; J = 0.9 K_T value (0.184) proves that there was an increase in K_T value. While Open propeller when J = 0.1 value $10K_Q$ 0.972; J = 0.5 value $10K_Q$ 0.700; J = 0.9 $10K_Q$ value (0.351) compared to PBCF when J = 0.1 $10K_Q$ value 0.962; J = 0.5 value $10K_Q$ 0.700; J = 0.9 value of $10K_Q$ (0.389) indicates a decrease in value of $10K_Q$ on the open propeller and PBCF. Then the comparison is seen from B4-70 propeller without PBCF Convergent η_0 value when J = 0.1 value η_0 0.086; J = 0.5 value η_0 0.421; J = 0.9 value η_0 (0.647) compared to PBCF when J = 0.1 value η_0 0.087; J = 0.5 value η_0 0.424; J = 0.9 value η_0 0.677 explains that with the use of PBCF the higher the value of J, the greater the increase in η_0 value. Meanwhile, between CFD and the experiment can be seen from Table 6 and Table 7, the highest K_T value is in CFD, which is 0.570 when J = 0, then the highest $10K_Q$ value is in CFD, which is 1.036 when J (0), and the highest η_0 value is in CFD, which is 0.677 in J = 0.9.

Table 5
CFD results for B4-70 propeller without PBCF Convergent

J	K_T	$10K_Q$	Efficiency
0.0	0.562	1.045	0.000
0.1	0.527	0.972	0.086
0.2	0.500	0.919	0.173
0.3	0.463	0.855	0.258
0.4	0.418	0.780	0.341
0.5	0.370	0.700	0.421
0.6	0.319	0.616	0.495
0.7	0.267	0.530	0.561
0.8	0.213	0.441	0.615
0.9	0.159	0.351	0.647
1.0	0.104	0.261	0.637

Table 6
Experimental results for B4-70 propeller with PBCF Convergent

J	K_T	$10K_Q$	Efficiency
0.0	0.570	1.036	0.000
0.1	0.526	0.962	0.087
0.2	0.512	0.929	0.175
0.3	0.464	0.851	0.260
0.4	0.434	0.798	0.346
0.5	0.373	0.700	0.424
0.6	0.339	0.641	0.505
0.7	0.272	0.534	0.567
0.8	0.236	0.473	0.634
0.9	0.184	0.389	0.677
1.0	0.129	0.298	0.686

Table 7
Experimental results for B4-70 propeller with PBCF Convergent

J	K_T	$10K_Q$	Efficiency
0.0	0.542	0.832	0.000
0.1	0.505	0.818	0.098
0.2	0.456	0.789	0.184
0.3	0.413	0.754	0.261
0.4	0.362	0.708	0.325
0.5	0.316	0.657	0.383
0.6	0.271	0.590	0.439
0.7	0.227	0.507	0.498
0.8	0.186	0.412	0.576
0.9	0.119	0.271	0.627
1.0	0.066	0.168	0.631

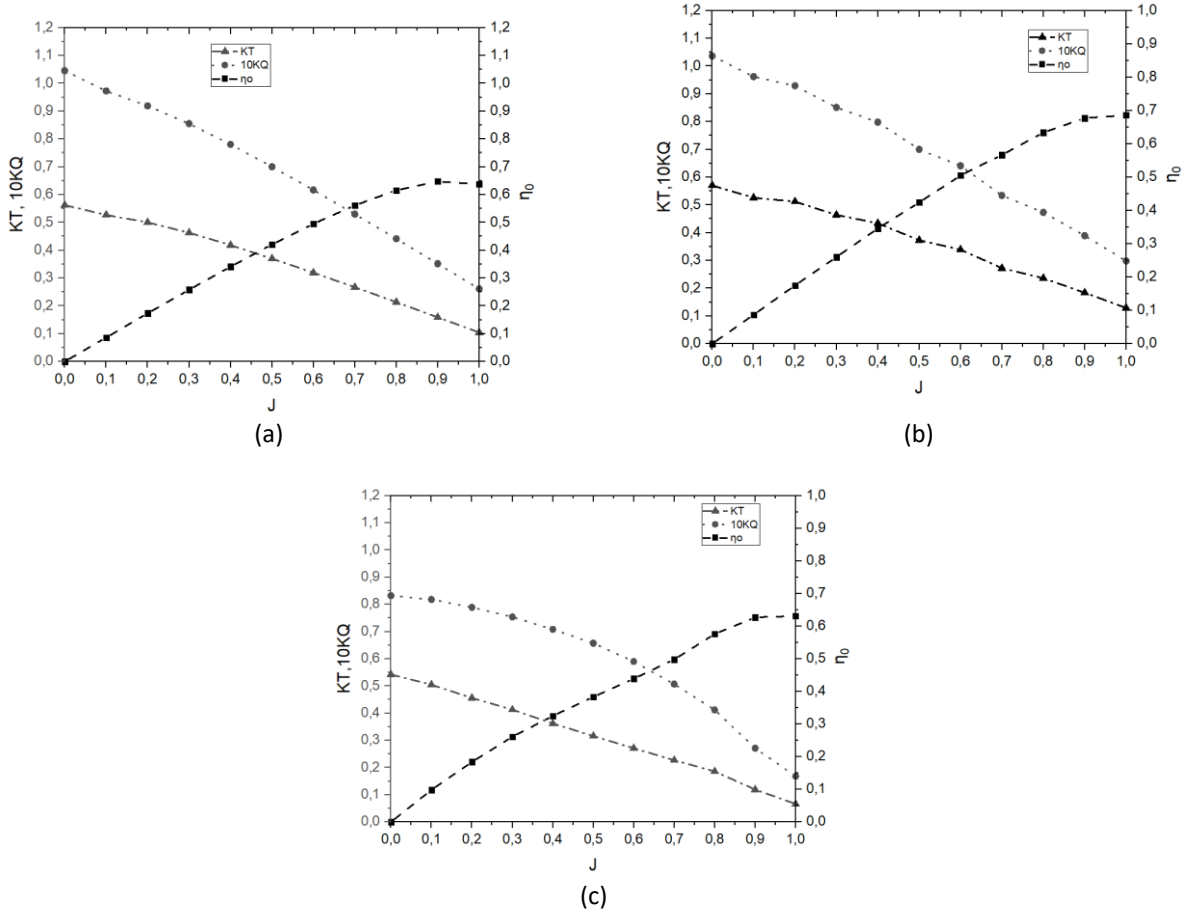

Fig. 8. Open water test diagram CFD and experiment for B4-70 propeller with and without PBCF Convergent (a) Open water test diagram CFD B4-70 without PBCF (b) Open water test diagram CFD B4-70 with PBCF (c) Open water test diagram experiment B4-70 with PBCF

The process of making the open water test graph refers to the Wageningen experimental graph where the graph shows the results of the K_T, $10K_Q$, and efficiency (η_0) values as shown in Figure 13. The open water test graph on the B4-70 propeller with BCF Convergent comes from the CFD simulation presented in Table 2 when J = 0.1 the K_T value is 0.526 decreases when J = 0.5 K_T is 0.373 to the lowest at J = 1.0 K_T 0.129 and has the same trend when J = 0.1 has a value of $10K_Q$ 0.962 also decreases when J = 0.5 has a value of $10K_Q$ 0.700 to the lowest at J = 1.0 a value of $10K_Q$ 0.298. However, η_0 value, on the other hand, is the lowest η_0 value when J = 0.1 increases at J = 0.5 with an η_0 of 0.424, the peak η_0 value is 0.686 when J = 1.0. It can be concluded on the B4-70 propeller with default Convergent boss cap fins that at low speed η_0 value is also low but K_T and $10K_Q$ are high, while the highest efficiency is J = 1.0 [21].

The pressure visualization of the B4-70 Propeller without PBCF as shown in Figure 9 corroborates the results of the CFD simulation in Table 5 and Figure 13. The results of the tables and graphs show that at low speeds J = 0 has a high K_T value of 0.562, and at moderate speeds J = 0.5 K_T value is 0.370; while at high speeds J = 0.9 the value of K_T is 0.159. In the boss cap fins, there is a large pressure when J = 0.1 ≥1000 Pa, while J = 0.5 is ≥1000 Pa, but the pressure value is small when J = 0.9 is ≥1000 Pa. In this study, the B4-70 propeller without PBCF experienced great pressure at low-speed J = 0.1 to medium-speed J = 0.5, so a solution was needed to reduce pressure.

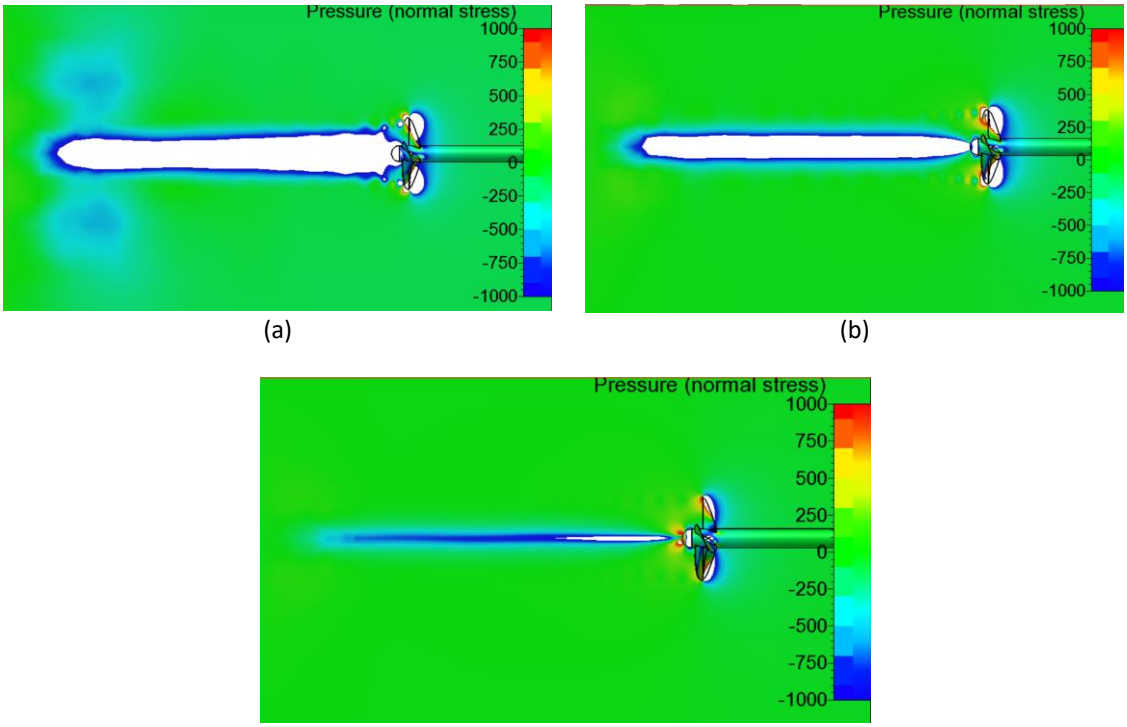

Fig. 9. Visualization of pressure B4-70 propeller without PBCF (a) Pressure without PBCF at J = 0.1 (b) Pressure without PBCF at H = 0.5 (c) Pressure without PBCF at J = 0.9

The visualization of the pressure Propeller B4-70 as shown in Figure 10 with straight boss cap fins strengthens the CFD simulation results in Table 5 and Figure 13. The results of the tables and graphs show that when J = 0.1 the K_T value is 0.526 it decreases when J = 0.5 K_T is 0.373 to lowest at J = 1.0 K_T 0.129. In the boss cap fins, there is a large pressure when J = 0.1 ≥1000 Pa, while J = 0.5 ≥1000 Pa, but the pressure value is small when J = 0.9 is ≥500 Pa. In this study, the Propeller B4-70 with PBCF convergent experienced a large pressure at low speeds J = 0.1 to J = 0.5, so a solution was needed to reduce pressure.

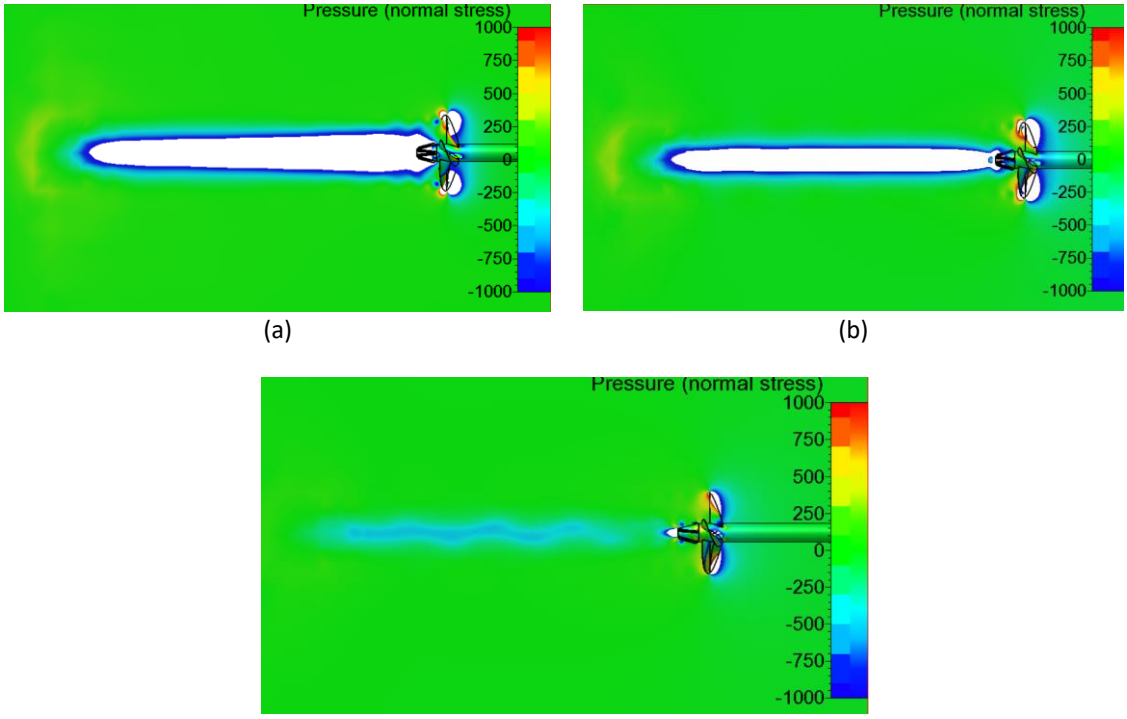

Fig. 10. Visualization of pressure propeller B4-70 with PBCF Convergent (a) Pressure PBCF Convergent at J = 0.1 (b) Pressure PBCF Convergent at J = 0.5 (c) Pressure PBCF Convergent at J = 0.9

The visualization of the velocity of the B4-70 Propeller without PBCF as shown in Figure 11 corroborates the results of the CFD simulation for the pressure value. In the boss cap fins, there is a large pressure when J = 0.1 ≥1000 Pa, while J = 0.5 is ≥1000 Pa, but the pressure value is small when J = 0.9 is ≥1000 Pa. In this study, the B4-70 propeller without PBCF experienced great pressure at low-speed J = 0.1 to medium-speed J = 0.5, so a solution was needed to reduce pressure. The visualization of the velocity of the B4-70 Propeller without PBCF strengthens the CFD simulation results for the pressure value. Starting from J = 0.1 in the blade section, the induce axial velocity is 2 m/s to 3 m/s, but in the boss cap propeller, flow occurs at speeds of 0 m/s to 1 m/s. Whereas in the J = 0.5 blade section the induce axial velocity is 2 m/s to 3 m/s and in the propeller cap boss section the flow occurs at 0 m/s to 2 m/s. Meanwhile, when J = 0.9 is in the blade section the induce axial velocity is 2 m/s to 3 m/s, however, in the boss cap propeller section, flow occurs with speeds of 0 m/s to 3 m/s. The conclusion on the B4-70 propeller without PBCF is that if the value of J (advanced coefficient) is higher, the flow velocity increases in the boss cap, but the flow velocity in the blade propeller remains the same. So a solution is needed to overcome the increase in flow velocity in the boss cap.

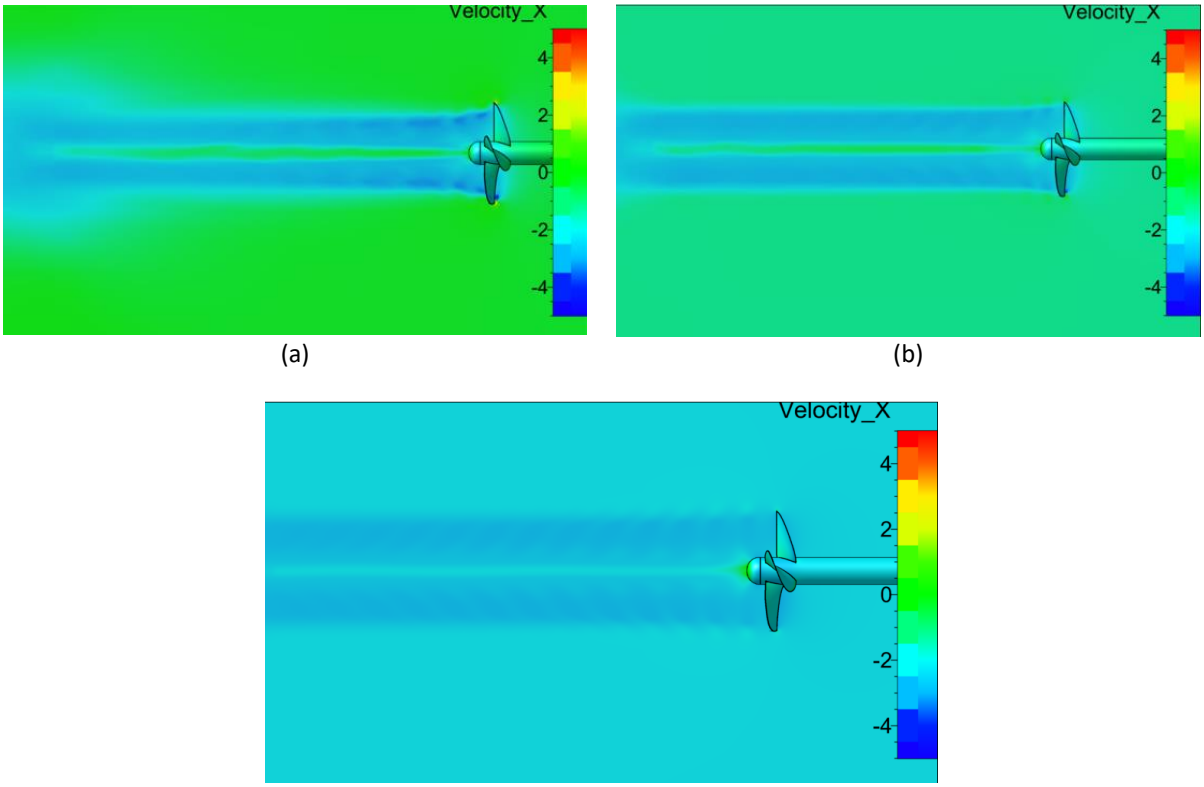

Fig. 11. Visualization of velocity B4-70 propeller without PBCF (a) Velocity without PBCF at J = 0.1 (b) Velocity without PBCF at J = 0.5 (c) Velocity without PBCF at J = 0.9

The B4-70 Propeller velocity visualization with boss cap fins convergent as shown in Figure 12 strengthens the CFD simulation results for the pressure value on the part of the boss cap fins, there is a large pressure when J = 0.1 ≥1000 Pa, while J = 0.5 ≥1000 Pa, but the pressure value is small when J = 0.9 is ≥500 Pa. In this study, the Propeller B4-70 with PBCF convergent experienced a large pressure at low speeds J = 0.1 to J = 0.5, so a solution was needed to reduce pressure. The visualization of the velocity of the Propeller B4-70 with the boss cap fins convergent strengthens the CFD simulation results on the pressure value. Starting from J = 0.1 in the blade section, the induce axial velocity is 2 m/s to 3 m/s, but in the boss cap propeller, flow occurs with speeds of 3 m/s to 5 m/s. Whereas in the J = 0.5 blade section the induce axial velocity is 2 m/s to 3 m/s and in the propeller cap boss section the flow occurs at 1 m/s to 2 m/s. Meanwhile, when J = 0.9 is in the blade section the induce axial velocity is 2 m/s to 3 m/s, however, in the boss cap propeller section, reverse flow occurs with a speed of 0 m/s to 1 m/s. The conclusion on the B4-70 propeller with PBCF convergent is obtained if the value of J (advanced coefficient) is higher, the flow velocity decreases in the boss cap and the flow velocity in the propeller blade decreases. So a solution is needed to overcome the increase in flow velocity in the boss cap.

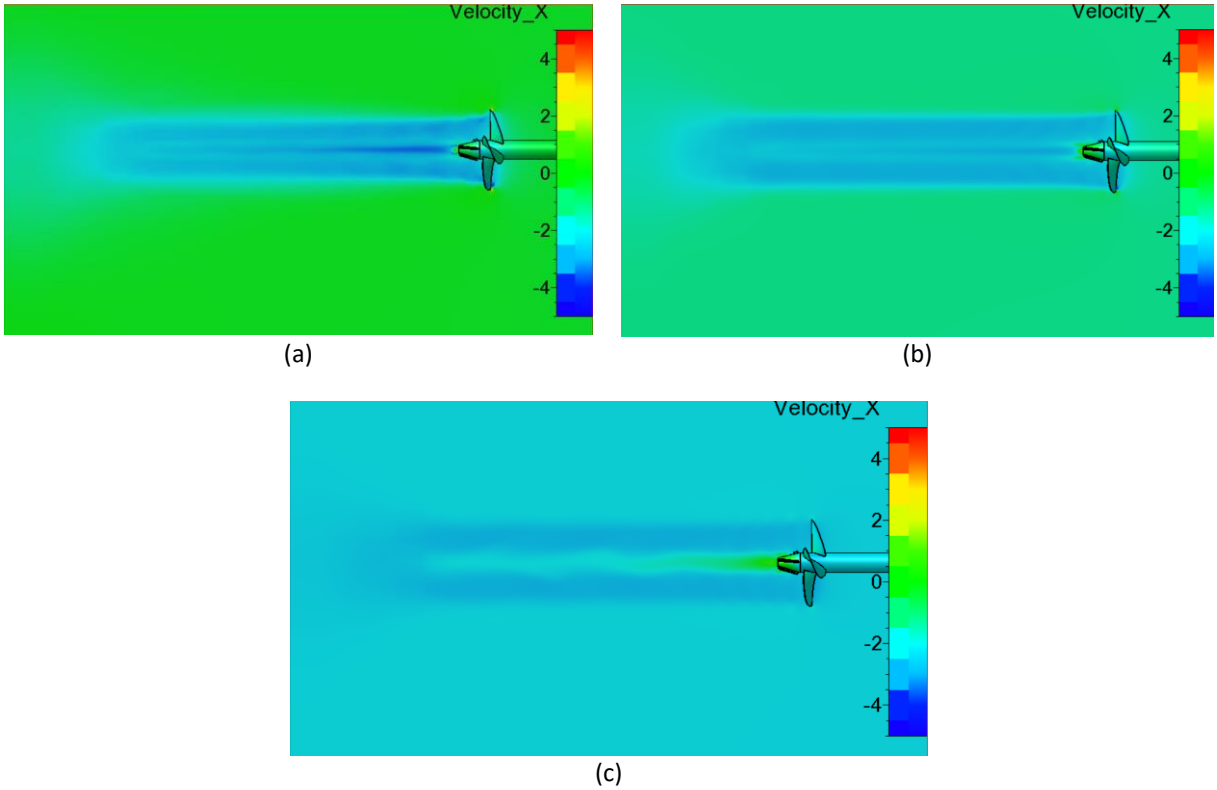

Fig. 12. Visualization of velocity B4-70 propeller with PBCF (a) Velocity PBCF Convergent at j = 0.1 (b) Velocity PBCF Convergent at J = 0.5 (c) Velocity PBCF Convergent at J = 0.9

The results of a comparative investigation between B4-70 Propeller with and without PBCF can be seen in Figure 13, namely, the value of K_T PBCF increases from J = 0.8 to J = 1.0 with the use of PBCF experiencing an increase in thrust by 10% to 24%, but $10K_Q$ value at B4-70 with PBCF experiencing decrease when J = 0.8 to J = 1.0 of 7% to 14% proving that the increase in K_T value is greater than $10K_Q$ value by installing PBCF, also η_0 value at J = 0.8 to J = 1.0 increases by 3 % to 8%, So it can be concluded that an B4-70 propeller without PBCF when added to ESD in the form of PBCF can increase the value of propeller η_0 when J is high, from J = 0.8 to J = 1.0 [22].

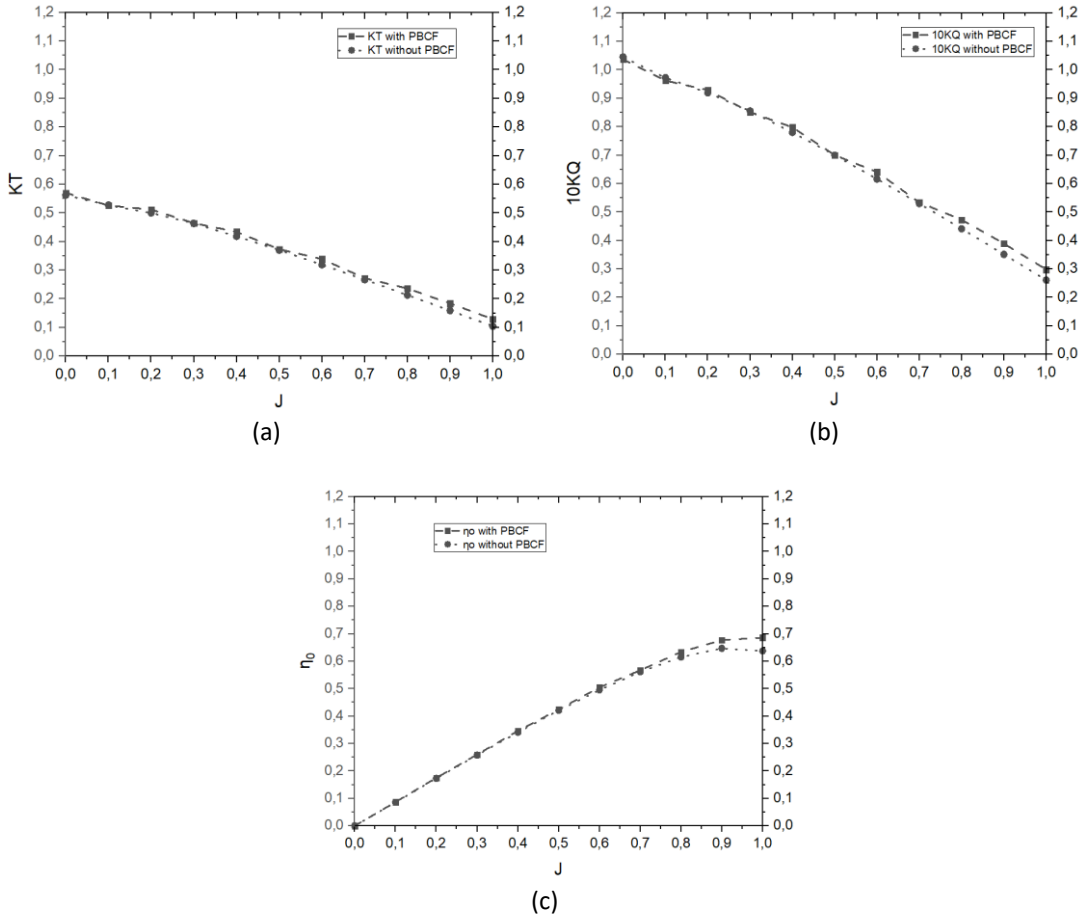

Fig. 13. Comparison Open Water Test B4-70 Propeller between with and without PBCF (a) K_T value CFD between with and without PBCF (b) $10K_Q$ Value CFD between with and without PBCF (c) Efficiency value CFD between with and without PBCF

The results of the investigation of comparative cases as shown in Figure 14 between CFD and Experiments from B4-70 propellers with PBCF Convergence show that several phenomena are occurred. On the $10K_Q$ graph, The first phenomenon shows the distance between J = 0 to J = 0.5 looking stretched, while J = 0.5 to J = 0.7 looks tighter. J = 0.7 to J = 1.0 width is starting to be larger, so further research is needed for torque. The second phenomenon 2 for small J values can be seen in the K_T values on CFD and experiments, proving that the vane flow at small J can be modeled numerically very well [23]. The last phenomenon of B4-70 propellers with PBCF with a convergent boss cap shape with a slope of 15 degrees shows an increase in efficiency was also shown in a study conducted by Abar *et al.,* [24], regarding the angle of inclination of the convergent boss cap of 15 degrees [25]. So that the overall calculation using the CFD approach can still be relied upon to complete as is the case in this paper.

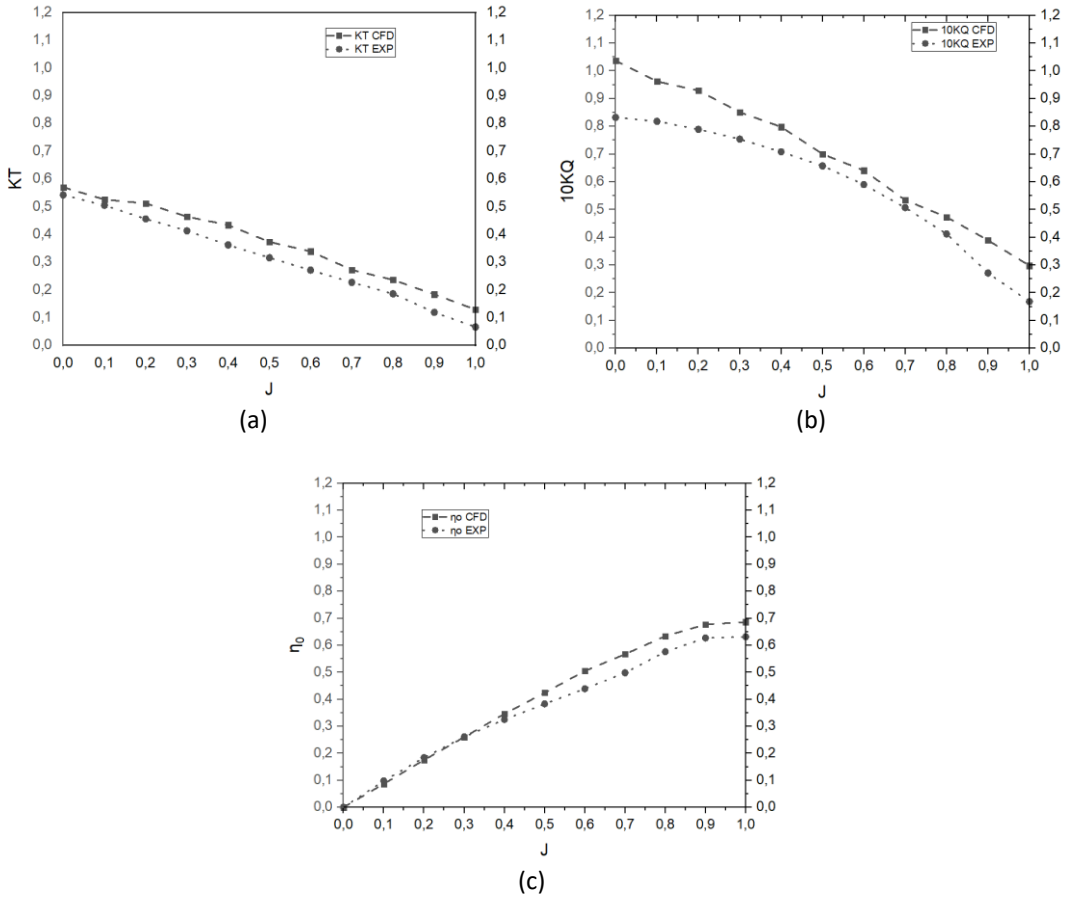

Fig. 14. Comparison open water test B4-70 Propeller between CFD and experiment (a) KT value between CFD and experiment (b) 10kQ value between CFD and experiment (c) Efficiency value between CFD and experiment

4. Conclusions

The Reynolds Averaged Navier Stokes Equation (RANSE) was used in this study, which was validated with experimental data from the open water test model. The B4-70 propeller design was created to investigate the effect of ESD on propeller efficiency, and it was then used to assess the effect of PBCF. On a model scale, CFD analysis was performed. The study's findings include a design that can be used for market ESD analysis.

The results of the investigation of comparative cases between CFD and Experiments from B4-70 propellers with PBCF Convergence, it appears that between CFD and Experiments, several phenomena are seen. i) The B4-70 Propeller without PBCF high Pressure at J = 0.1 - 0.9, but with boss cap fins can reduce pressure at high-speed J = 0.9, so further research is needed to low-speed J = 0.1 - 0.5; ii) Visualization of velocity on propeller B4-70 without PBCF shows an increase in flow velocity in the boss cap fins when J = 0 to J = 0.9, whereas the induce axial velocity in the blade propeller is the same and propeller B4-70 with PBCF decreases in speed in the boss cap fins when J = 0 to J = 0.9, however the induce axial velocity in the blade propeller is the same; iii) Comparison of open propeller and PBCF shows that using PBCF there is an increase in the K_T value at high speed of 10% to 24% and a decrease in the $10K_Q$ value on PBCF from J = 0.8 to J = 1.0 of 7% to 14%, however η_0 value at J = 0.8 to J = 1.0 increased by 3% to 8%, explaining that the use of PBCF when the higher the value of J, the greater the increase in η_0 value; iv) B4-70 propeller with PBCF with converging boss cap shape with

15-degree slope exhibits increased efficiency. So that the overall calculation using the CFD approach can still be relied upon to complete as is the case in this paper.

Acknowledgment
The authors wished to thank Institut Teknologi Sepuluh Nopember for funding the research through a research scheme known as “Research for Doctoral Dissertation” under contract number: 1566/PKS/ITS/2022. The authors acknowledge the facilities, and scientific and technical support from Hydrodynamics Laboratory, National Research, and Innovation Agency. The first author would like to express gratitude in particular to Diponegoro University for providing the doctoral degree study funding. Sutiyo of the Hang Tuah University, Surabaya, assisted with the CFD work and the authors are grateful for his help.

References

[1] Mahdiyan, Alinda. "Perekonomian Dunia Diprediksi Akan Dihantam Resesi Tahun 2023, Bagaimana Dengan Pembangunan Infrastruktur?" Kementrian Keuangan Republik Indonesia, 2022.
[2] Hansen, Hans Richard, Tom Dinham-Peren, and Takeo Nojiri. "Model and full scale evaluation of a ‘propeller boss cap fins’ device fitted to an Aframax tanker." In *Second International Symposium on Marine Propulsors*. 2011.
[3] Mewis, Friedrich. "A novel power-saving device for full-form vessels." In *First International Symposium on Marine Propulsors, SMP*, vol. 9. 2009.
[4] Celik, Ishmail B., Urmila Ghia, Patrick J. Roache, and Christopher J. Freitas. "Procedure for estimation and reporting of uncertainty due to discretization in CFD applications." *Journal of fluids Engineering-Transactions of the ASME* 130, no. 7 (2008). https://doi.org/10.1115/1.2960953
[5] MEPC, IMO. "1/Circ. 684 guidelines for voluntary use of the ship energy efficiency operational indicator (EEOI)." *International Maritime Organization: London, UK* (2009).
[6] Adietya, Berlian Arswendo, I. Ketut Aria Pria Utama, and Wasis Dwi Aryawan. "CFD Analysis into the Effect of using Propeller Boss Cap Fins (PBCF) on Open and Ducted Propellers, Case Study with Propeller B-Series and Kaplan-Series." *CFD Letters* 14, no. 4 (2022): 32-42. https://doi.org/10.37934/cfdl.14.4.3242.
[7] Niknahad, Ali. "Numerical study and comparison of turbulent parameters of simple, triangular, and circular vortex generators equipped airfoil model." *Journal of Advanced Research in Numerical Heat Transfer* 8, no. 1 (2022): 1-18.
[8] Darsono, Febri Budi, Rahmad Doni Widodo, and Akhmad Nurdin. "Analysis Of the Effect of Flow Rate and Speed on Four Blade Tubular Water Bulb-Turbine Efficiency Using Numerical Flow Simulation." *Journal of Advanced Research in Fluid Mechanics and Thermal Sciences* 90, no. 2 (2021): 1-8. https://doi.org/10.37934/arfmts.90.2.18.
[9] Wallin, Stefan. *Engineering turbulence modelling for CFD with focus on explicit algebraic Reynolds stress models*. Stockholm, Sweden: Royal Institute of Technology, Department of Mechanics, 2000.
[10] Xing, Ling Hang., Geng Bin Huang, and Min Yan. "Numerical Simulation of 3D Density Flow by an Improved EASM Model." *Procedia Environmental Sciences* 10 (2011): 753-758. https://doi.org/10.1016/j.proenv.2011.09.122.
[11] Mizzi, Kurt, Yigit Kemal Demirel, Charlotte Banks, Osman Turan, Panagiotis Kaklis, and Mehmet Atlar. "Design optimisation of Propeller Boss Cap Fins for enhanced propeller performance." *Applied Ocean Research* 62 (2017): 210-222. https://doi.org/10.1016/j.apor.2016.12.006.
[12] Kawamura, Takafumi, Kazuyuki Ouchi, and Takeo Nojiri. "Model and full scale CFD analysis of propeller boss cap fins (PBCF)." *Journal of marine science and technology* 17 (2012): 469-480. https://doi.org/10.1007/s00773-012-0181-2.
[13] Versteeg, Henk Kaarle, and Weeratunge Malalasekera. *An introduction to computational fluid dynamics: the finite volume method*. Pearson education, 2007.
[14] Numeca International - Cadence Design Systems. n.d. “FINEMarine-Theory-Guide.”
[15] Ismail, Iman Fitri, Akmal Nizam Mohammed, Bambang Basuno, Siti Aisyah Alimuddin, and Mustafa Alas. "Evaluation of CFD Computing Performance on Multi-Core Processors for Flow Simulations." *Journal of Advanced Research in Applied Sciences and Engineering Technology* 28, no. 1 (2022): 67-80. https://doi.org/10.37934/araset.28.1.6780.
[16] Abobaker, Mostafa, Sogair Addeep, Lukmon O. Afolabi, and Abdulhafid M. Elfaghi. "Effect of Mesh Type on Numerical Computation of Aerodynamic Coefficients of NACA 0012 Airfoil." *Journal of Advanced Research in Fluid Mechanics and Thermal Sciences* 87, no. 3 (2021): 31-39. https://doi.org/10.37934/arfmts.87.3.3139.
[17] Andersson, Bengt, Ronnie Andersson, Love Håkansson, Mikael Mortensen, Rahman Sudiyo, and Berend Van Wachem. *Computational fluid dynamics for engineers*. Cambridge university press, 2011.

[18] Ramli, Muhammad Ridzwan, Wan Mazlina Wan Mohamed, Hamid Yusoff, Mohd Azmi Ismail, Ahmed Awaludeen Mansor, Azmi Hussin, and Aliff Farhan Mohd Yamin. "The Aerodynamic Characteristics Investigation on NACA 0012 Airfoil with Owl's Wing Serrations for Future Air Vehicle." *Journal of Advanced Research in Fluid Mechanics and Thermal Sciences* 102, no. 1 (2023): 171-183. https://doi.org/10.37934/arfmts.102.1.171183.

[19] "Data Acquisition (DAQ) Systems, Devices & Software. "

[20] ITTC. 2002. "Propulsor Open Water Test. " *International Towing Tank Conference (ITTC) Testing and Extrapolation Methods Propulsion*.

[21] Ghassemi, Hassan, Amin Mardan, and Abdollah Ardeshir. "Numerical analysis of hub effect on hydrodynamic performance of propellers with inclusion of PBCF to equalize the induced velocity." *Polish Maritime Research* 19, no. 2 (2012): 17-24. https://doi.org/10.2478/v10012-012-0010-x.

[22] Gaggero, Stefano. "Design of PBCF energy saving devices using optimization strategies: A step towards a complete viscous design approach." *Ocean Engineering* 159 (2018): 517-538. https://doi.org/10.1016/j.oceaneng.2018.01.003.

[23] Cheng, Ma, Hao-peng Cai, Zheng-fang Qian, and C. H. E. N. Ke. "The design of propeller and propeller boss cap fins (PBCF) by an integrative method." *Journal of Hydrodynamics, Ser. B* 26, no. 4 (2014): 586-593. https://doi.org/10.1016/S1001-6058(14)60066-4.

[24] Abar, Insanu Abdilla Cendikia, and I. K. A. P. Utama. "Effect of the incline angle of propeller boss cap fins (PBCF) on ship propeller performance." *International Journal of Technology* 10, no. 5 (2019): 1056-1064. https://doi.org/10.14716/ijtech.v10i5.2256.

[25] Katayama, Kenta, Yoshihisa Okada, and Akinori Okazaki. "Optimization of the Propeller with ECO-Cap by CFD." In *Proceedings of the International Symposium on Marine Propulsors (SMP'15), Austin, TX, USA*, vol. 31. 2015.